Supporting Information for

# Monolithic Gyroidal Mesoporous Mixed Titanium-Niobium Nitrides

*Spencer W. Robbins,[†‡] Hiroaki Sai,[‡] Francis J. DiSalvo,[†] Sol M. Gruner,[⊥§#] Ulrich Wiesner[‡]**

[†]Department of Chemistry and Chemical Biology, [‡]Department of Materials Science and Engineering, [⊥]Department of Physics, [§]Cornell High Energy Synchrotron Source (CHESS), [#]Kavli Institute at Cornell for Nanoscale Science, Cornell University, Ithaca, New York 14853

*Corresponding author: ubw1@cornell.edu

**Table S1.**

| Component | **$M_n$ (kg/mol)** | **Wt%** | **Vol%** | **PDI** |
|---|---|---|---|---|
| **ISO1** | 59.6 | - | - | 1.09 |
| **PI** | 17.7 | 29.7% | 33.3% | 1.09 |
| **PS** | 37.4 | 62.8% | 60.2% | - |
| **PEO** | 4.5 | 7.5% | 6.5% | - |

| Component | **$M_n$ / (kg/mol)** | **Wt%** | **Vol%** | **PDI** |
|---|---|---|---|---|
| **ISO2** | 69.0 | - | - | 1.04 |
| **PI** | 20.4 | 29.6% | 33.1% | 1.02 |
| **PS** | 44.7 | 64.8% | 62.0% | - |
| **PEO** | 3.9 | 5.6% | 4.9% | - |

| Component | **$M_n$ / (kg/mol)** | **Wt%** | **Vol%** | **PDI** |
|---|---|---|---|---|
| **ISO3** | 63.8 | - | - | 1.03 |
| **PI** | 18.7 | 29.3% | 32.8% | 1.02 |
| **PS** | 40.5 | 63.6% | 61.0% | - |
| **PEO** | 4.6 | 7.1% | 6.3% | - |

**Table S2.**

**$d_{100}$-spacings in nanometers for ISO1 and ISO2 (8:2 Ti:Nb) and ISO3 (1:1 Ti:Nb)**

| | ISO1 | ISO2 | ISO3 |
|---|---|---|---|
| **Hybrid** | 48.9 | 52.4 | 55.9 |
| **Oxide** | 37.5 | 40.7 | 42.3 |
| **Nitride** | 36.1 | 39.1 | 37.9 |

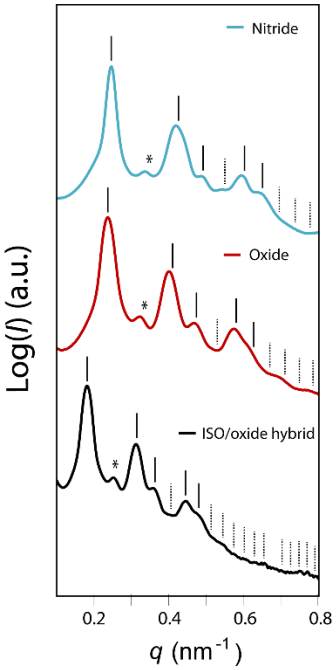


**Figure S1.** Azimuthally integrated small angle X-ray scattering patterns of the ISO1/oxide hybrid (bottom, black), calcined freestanding oxide (middle, red), and freestanding nitride (top, blue). The vertical lines indicate expected peak positions for the $G^A$ morphology. Dashed lines represent unobserved peaks and asterisks are centered at forbidden $(q/q_{100})^2 = 4$ peak positions that appear due to *z*-direction

compression. The $d_{100}$-spacings of the hybrid, oxide, and nitride are 48.9 nm, 37.5 nm, and 36.1 nm, respectively.

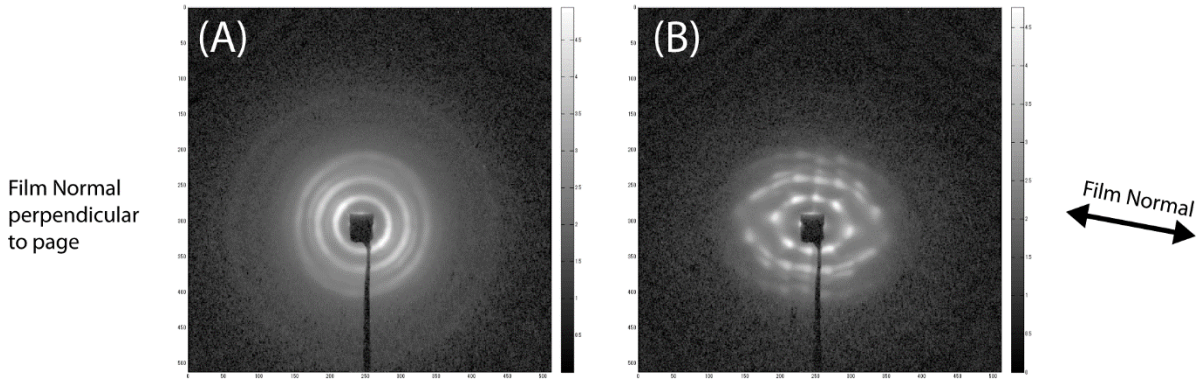


**Figure S2.** 2D SAXS patterns of an ISO2/oxide hybrid with incident X-rays parallel (A) and perpendicular (B) to the film normal. In (B), compression along the film normal direction, as well as clear texturing in the <110> direction parallel to the film normal, is observed.

## Additional conductivity measurements

ISO3 is a third triblock terpolymer with similar molar mass and composition to ISO1 and ISO2 (see Table S1) and was used to generate monolithic gyroidal nitrides with similar feature sizes and *d*-spacings as ISO1 and ISO2. These nitride monoliths materials were used for additional conductivity measurements as tabulated below.

ISO3 nitride materials were used to measure both powder and pellet conductivities. Powder conductivity under a pressure 200 psi was measured in an apparatus as described in a previous publication.[1] Pellets were pressed from powders of ground monoliths and pressed into a pellet under a pressure of 9000 psi in a die. The conductivity of the pellet was measured using the four point probe setup.

A monolithic nitride sample generated from ISO2 was also used for the four point probe conductivity measurements. The four point probe measurements were performed on a Cascade Microtech CPS-06 using tungsten carbide probe tips and a Keithley 2400 sourcemeter.

**Table S3.**

**Electrical Conductivity Measurements from ISO3-derived nitrides**

| | **Conductivity (S/cm)** |
|---|---|
| **Monolith** | ~5.2, ~9.3 |
| **Pellet (9000 psi)** | ~$6.3 \times 10^{-2}$ |
| **Powder (200 psi)** | ~$7.1 \times 10^{-4}$ |

The monoliths from ISO3 showed similar electrical conductivity to the ISO2 monolith, on the order of 1-10 S/cm. However, the measured powder and pellet conductivities were markedly lower than any of the monoliths. The higher pressure pellet did show higher conductivity than the low pressure powder, as expected. This disparity between monoliths and powders/pellets is likely due to poor particle-particle contact in the powders/pellets. In monoliths, the excellent 3D connectivity provides a continuous path for electrons and avoids the additive contact resistance from each particle-particle contact in the powders or pellets.

**Additional Figures**

Not shown here are closed off layers on the top and bottom of the film from bulk casting which have been observed in similar systems previously.[2]

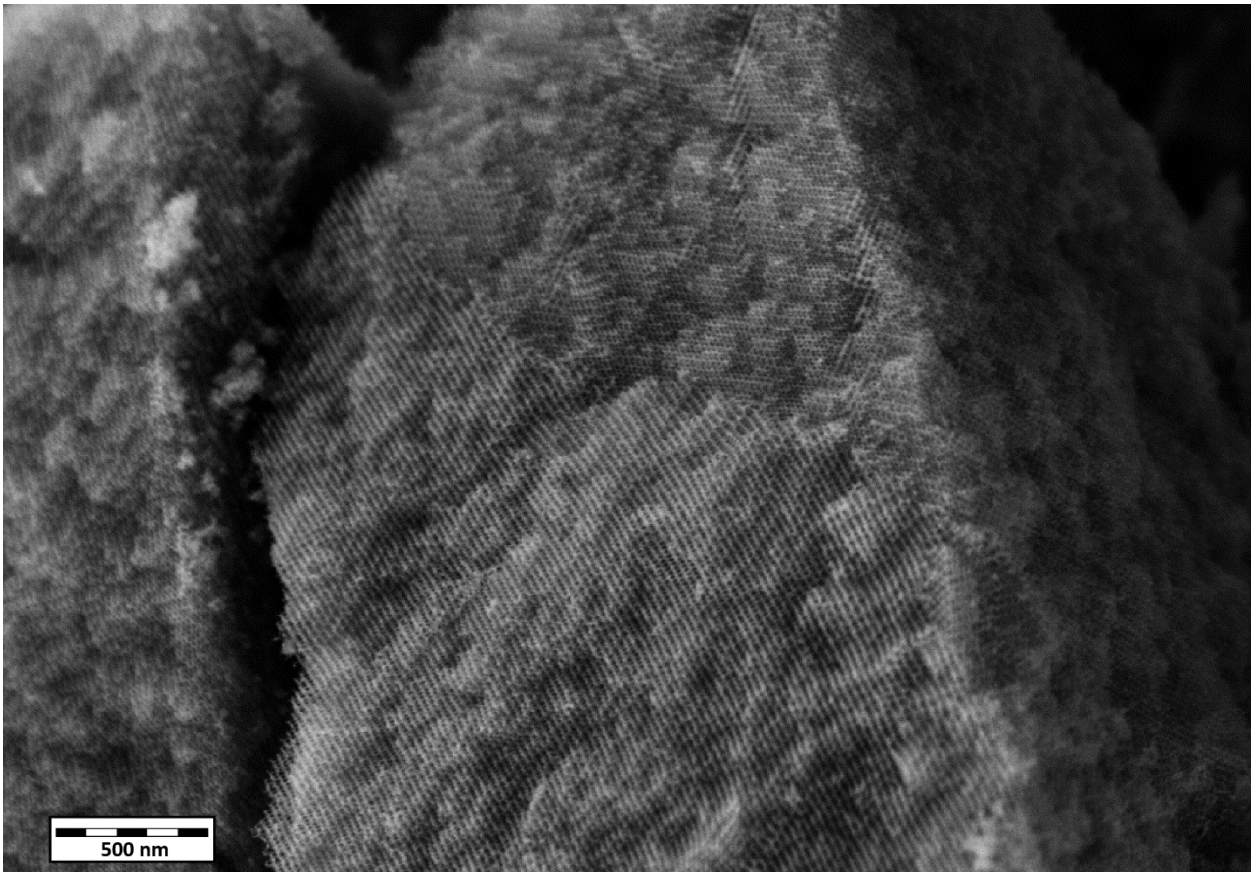


**Figure S3.** SEM image of $Ti_{0.8}Nb_{0.2}N$ from ISO1, showing fracture edges in a powder sample. Several grains of different orientations are evident.

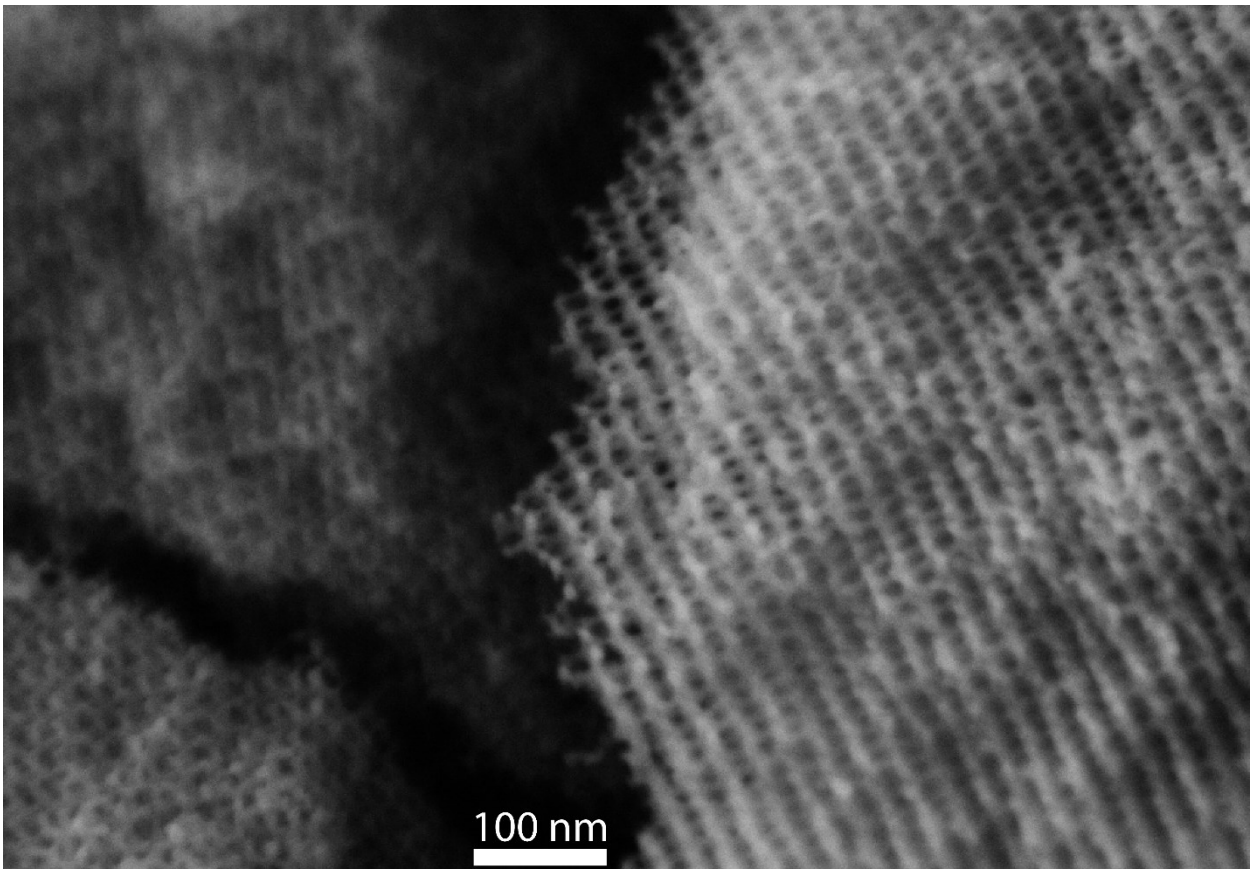


**Figure S4.** SEM image of $Ti_{0.8}Nb_{0.2}N$ from ISO1, showing fracture edges in a powder sample. Multiple layers of struts are evident along the edge.

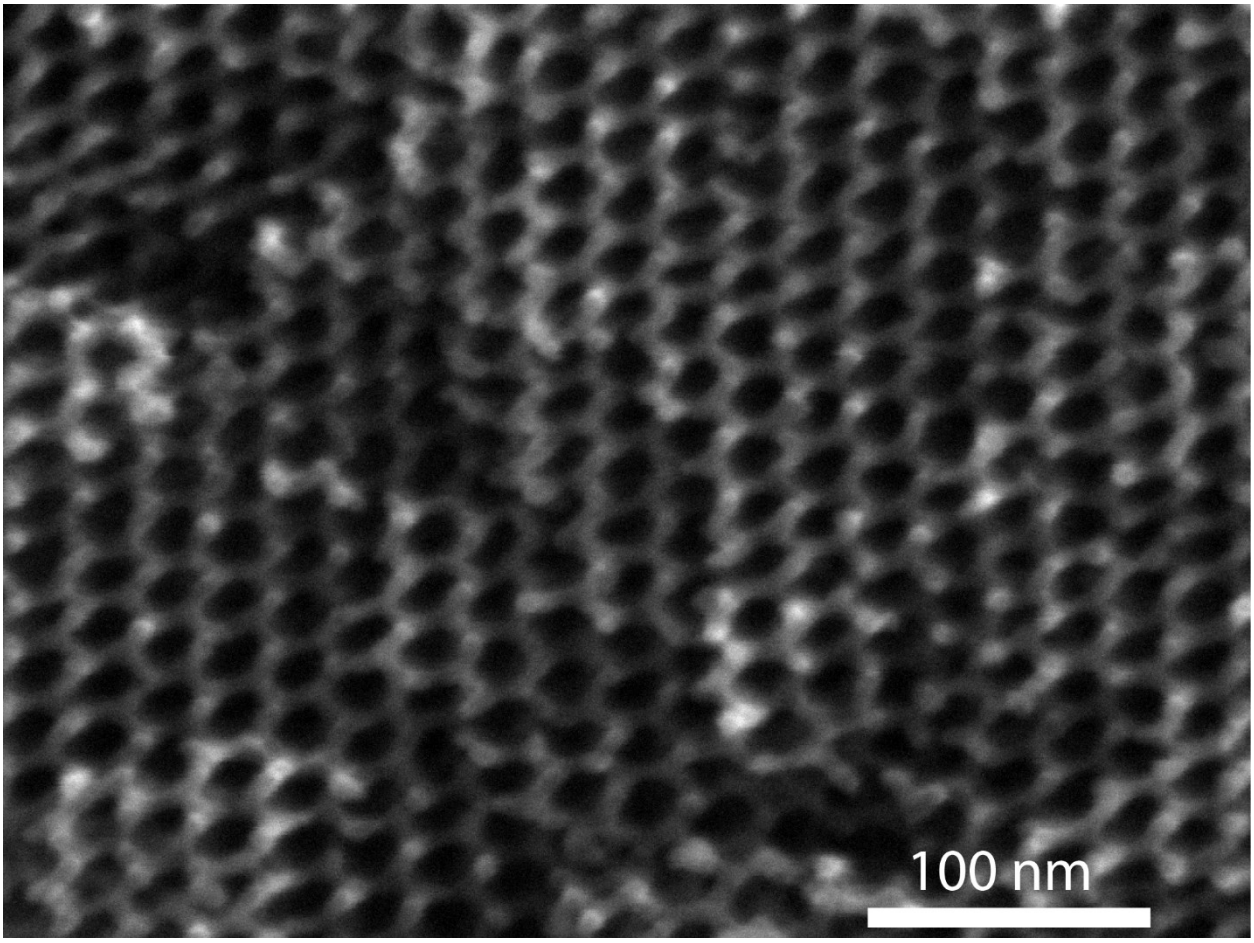


**Figure S5.** SEM image of $Ti_{0.8}Nb_{0.2}N$ from ISO2 showing structures consistent with the $G^A$ morphology.

**UV-vis-NIR Spectroscopy**

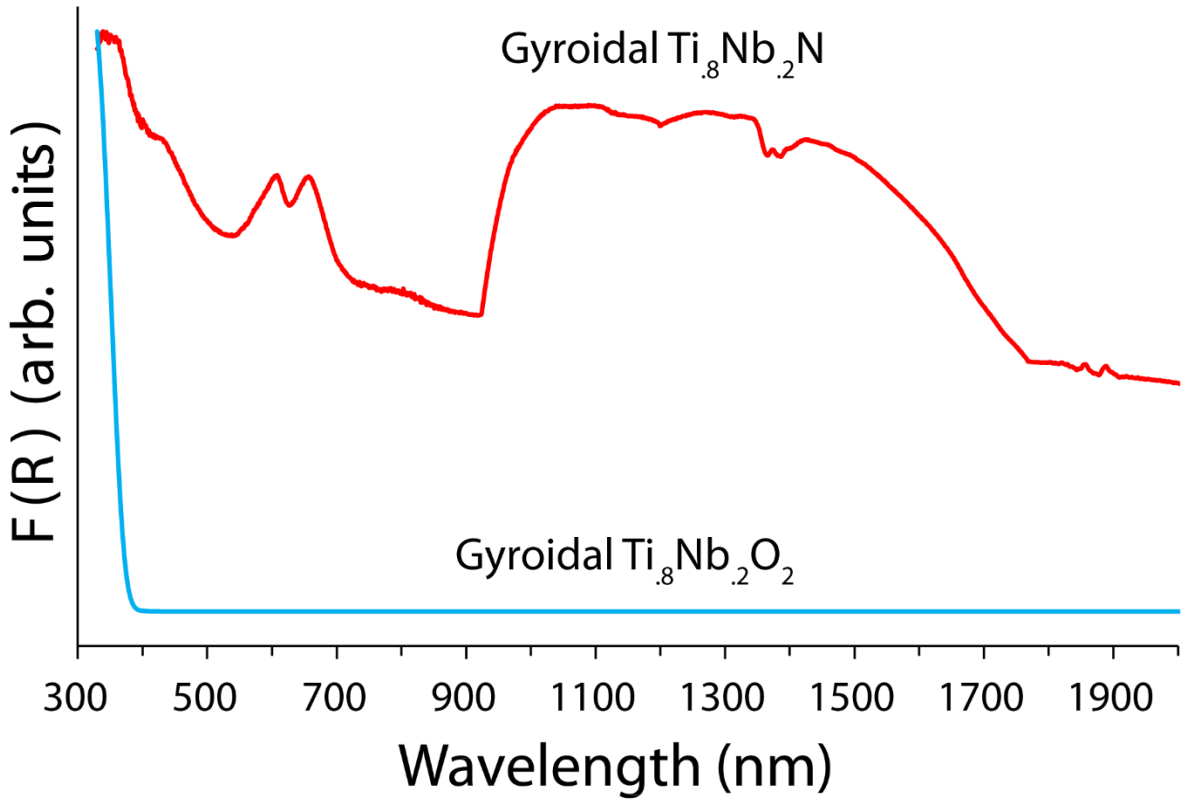


**Figure S6.**

Normalized UV-vis-NIR spectra of the Kubelka-Munk function as a function of wavelength for a powdered gyroidal $Ti_{0.8}Nb_{0.2}O_2$ (blue, bottom) and a powdered gyroidal $Ti_{0.8}Nb_{0.2}N$ (red, top). Lamp/grating switchover discontinuities were removed at 1200 nm and 800 nm.

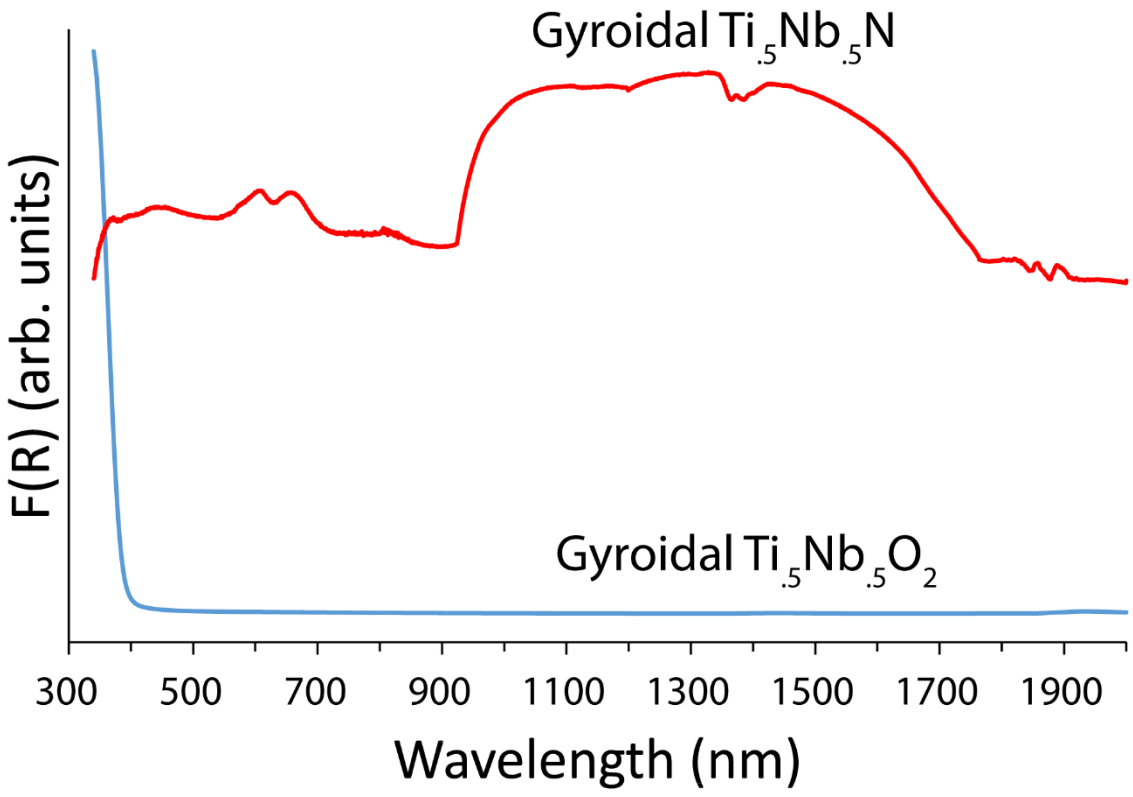


**Figure S7.** Normalized UV-vis-NIR spectra of the Kubelka-Munk function as a function of wavelength for a powdered gyroidal $Ti_{0.5}Nb_{0.5}O_2$ (blue, bottom) and a powdered gyroidal $Ti_{0.5}Nb_{0.5}N$ (red, top). Lamp/grating switchover discontinuities were removed at 1200 nm and 800 nm.

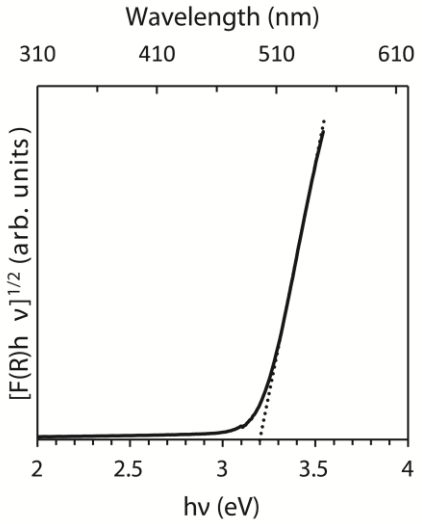


**Figure S8.** $[F(R)*h\nu]^{1/2}$ *vs*. hν plot and linear extrapolation to the x-axis for the powdered gyroidal $Ti_{0.8}Nb_{0.2}O_2$ sample. The x-intercept is at 3.20 eV, estimating the band gap of the oxide.

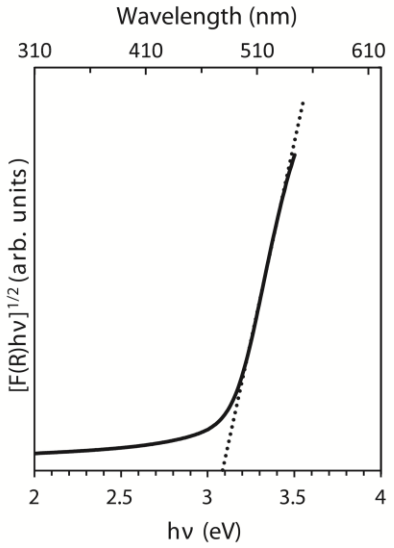


**Figure S9.** $[F(R)*h\nu]^{1/2}$ *vs*. hν plot and linear extrapolation to the x-axis for the powdered gyroidal $Ti_{0.5}Nb_{0.5}O_2$ sample. The x-intercept is at 3.09 eV, estimating the band gap of the oxide.

Powdered gyroidal oxide and nitride samples were characterized by UV-vis-NIR spectroscopy with an integrating sphere accessory on an Agilent Cary 5000 UV-vis-NIR using reflectance mode and is plotted as the Kubelka-Munk function against wavelength.[3] The powders were sandwiched between microglass slides for the measurements.

The white colored powder $Ti_{0.8}Nb_{0.2}O_2$ sample showed a characteristic absorption edge around 380 nm as shown in Figure S6, (bottom, blue). The band gap was estimated (assuming an indirect optical band gap) to be 3.20 eV by extrapolating the linear region of an $[F(R)*h\nu]^{1/2}$ *vs*. hν plot (where F(R) is the Kubelka-Munk function) to the x-intercept, shown in Figure S8.[3] This value is in good agreement with reported values of anatase $TiO_2$ [4,5] and $Ti_{1-x}Nb_xO_2$.[6,7] In comparison, the white colored powder $Ti_{0.5}Nb_{0.5}O_2$ showed a broadened absorption edge, which was not surprising since the material is amorphous. The band gap was estimated (assuming an indirect optical band gap) to be 3.09 eV by extrapolating the linear region of an $[F(R)*h\nu]^{1/2}$ *vs*. hν plot (where F(R) is the Kubelka-Munk function) to the x-intercept, shown in Figure S9.

The black colored powdered nitride samples showed dramatically different optical behavior (Fig. S6, S7, red). $Ti_{0.8}Nb_{0.2}N$ (Fig. S6) showed broad absorption across the measured spectrum with some defined features: two peaks around 610 and 665 nm and a significant absorption between 920 and 1700 nm. $Ti_{0.5}Nb_{0.5}N$ (Fig. S7) showed a similar broad absorption across the measured spectrum with some defined features: two peaks around 620 and 675 nm and a significant absorption between 920 and 1700 nm. The peaks around 620 and 675 are less intense than in $Ti_{0.8}Nb_{0.2}N$ and it also tends to absorb less at shorter wavelengths.

The color change from white wide band gap oxides to black and conducting nitrides is similar to that observed for $TiO_2$ which was nitrided to yield TiN.[5] The gyroidal nitride's optical behavior resembles the cubic nitride rather than a N-doped oxide, which is consistent with the XRD results.[5,8]

**Raman Spectroscopy**

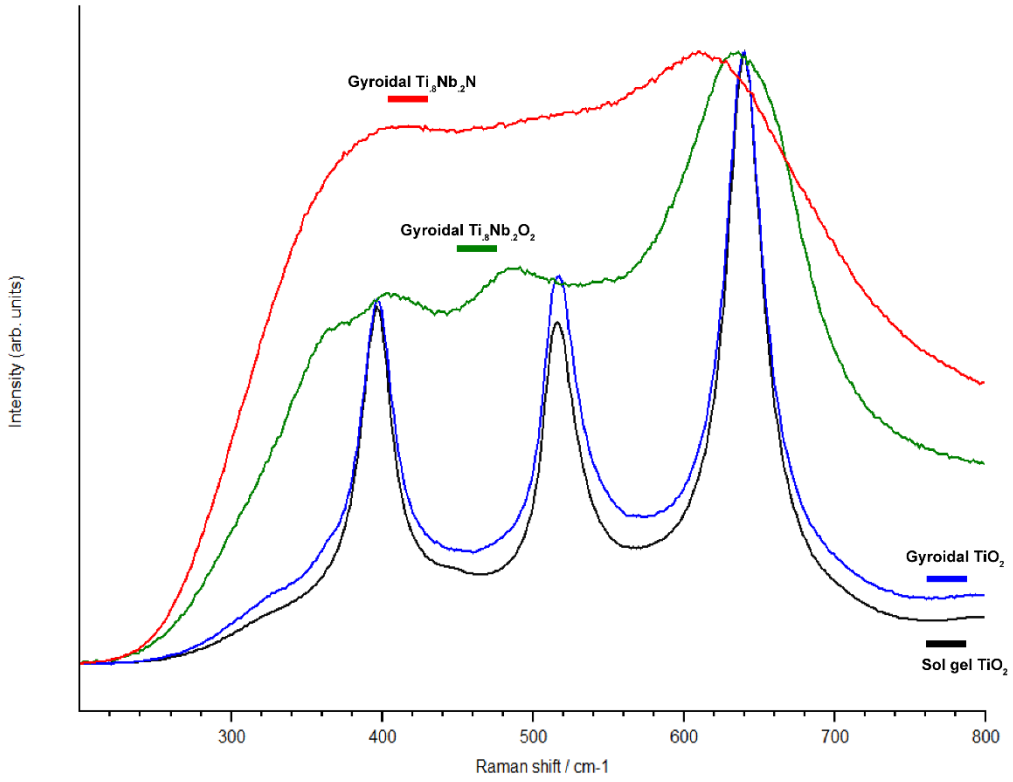


**Figure S10.** Normalized Raman spectra for non-structured $TiO_2$ (black, bottom), gyroidal $TiO_2$ (blue), gyroidal $Ti_{0.8}Nb_{0.2}O_2$ (green), and gyroidal $Ti_{0.8}Nb_{0.2}N$ (red, top).

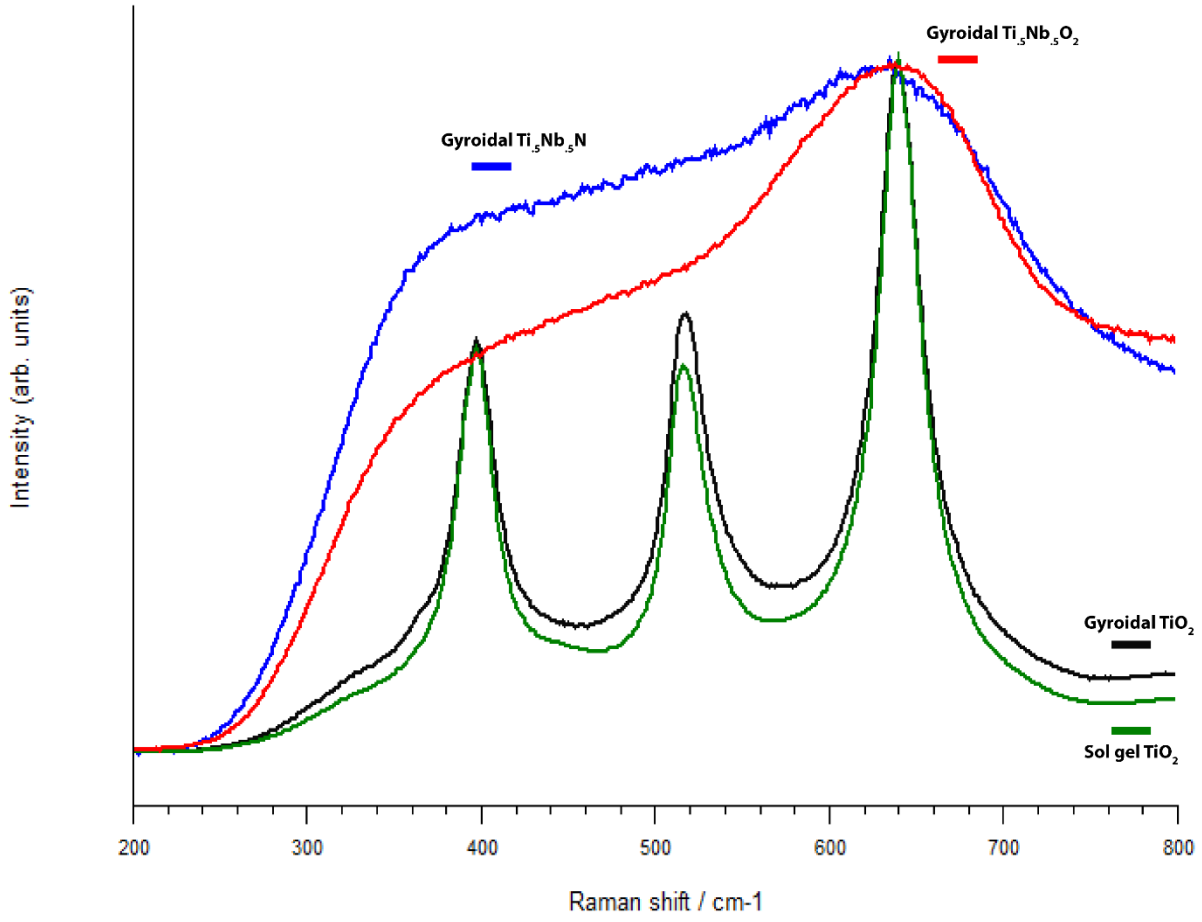


**Figure S11.** Normalized Raman spectra for non-structured $TiO_2$ (green, bottom), gyroidal $TiO_2$ (black), gyroidal $Ti_{0.5}Nb_{0.5}O_2$ (red), and gyroidal $Ti_{0.5}Nb_{0.5}N$ (blue, top).

We performed Raman spectroscopy measurements on the powders of the gyroidal oxide and gyroidal nitride samples on a Renishaw InVia Confocal Raman Microscope using a 488 nm laser and a 50x long working distance objective. The results are displayed in Figures S10 and S11.

To see the effects of Nb incorporation and nitriding, we first probed non-structured sol-gel derived anatase $TiO_2$ and gyroidal anatase $TiO_2$ (both crystalline). These showed strong scattering, as expected for crystalline materials, and are consistent with the well-defined expected bands for anatase.[6,9]

The gyroidal $Ti_{0.8}Nb_{0.2}O_2$ sample (Fig. S10) shows broad bands (due to amorphous oxide content), with most prominent anatase band observed around 640 $cm^{-1}$ which is expected for anatase $TiO_2$ and Nb-doped $TiO_2$[6] or niobia/titania composites.[9]

The shift of the broad band around 400 $cm^{-1}$ may be due to the incorporation of Nb in the anatase lattice.[6] However, the broad middle band near 485 $cm^{-1}$ is significantly shifted between expected positions for either anatase or rutile and could not be definitively identified.[9]

The gyroidal $Ti_{0.5}Nb_{0.5}O_2$ sample (Fig. S11) is amorphous and shows very broad bands, but the strongest band is still around 640 $cm^{-1}$.

After nitriding, both materials show very broad bands which are consistent with a cubic nitride like TiN or $Ti_{1-x}Nb_xN$ (both cubic rock salt structure), rather than a nitrogen doped $TiO_2$ or $Ti_{1-x}Nb_xO_2$.[5] Small grain sizes can also contribute to broad bands.[9] In cubic binary nitrides, first order scattering is forbidden, so scattering is predominantly derived from impurities and defects, resulting in the observed broad bands.[5,11,12] We speculate that oxygen[5] and Nb[12] content can shift the bands in the gyroidal $Ti_{0.8}Nb_{0.2}N$ samples.

**References**:


1. Subban, C. V.; Smith, I. C.; DiSalvo, F. J., Interconversion of Inverse Opals of Electrically Conducting Doped Titanium Oxides and Nitrides. *Small* **2012**, *8*, 2824-2832.

2. Stefik, M.; Wang, S.; Hovden, R.; Sai, H.; Tate, M. W.; Muller, D. A.; Steiner, U.; Gruner, S. M.; Wiesner, U., Networked and Chiral Nanocomposites from ABC Triblock Terpolymer Coassembly with Transition Metal Oxide Nanoparticles. *J. Mater. Chem.* **2012**, *22*, 1078-1087.

3. Geladi, P.; MacDougall, D.; Martens, H., Linearization and Scatter-Correction for Near-Infrared Reflectance Spectra of Meat. *Appl. Spectrosc.* **1985**, *39*, 491-500.

4. Beranek, R.; Kisch, H., Tuning the Optical and Photoelectrochemical Properties of Surface-Modified $TiO_2$. *Photochem. Photobiol. Sci.* **2008**, *7*, 40-48.

5. Zhang, Z.; Goodall, J. B. M.; Morgan, D. J.; Brown, S.; Clark, R. J. H.; Knowles, J. C.; Mordan, N. J.; Evans, J. R. G.; Carley, A. F.; Bowker, M., *et al.*, Photocatalytic Activities of N-Doped Nano-Titanias and Titanium Nitride. *J. Eur. Ceram. Soc.* **2009**, *29*, 2343-2353.

6. De Trizio, L.; Buonsanti, R.; Schimpf, A. M.; Llordes, A.; Gamelin, D. R.; Simonutti, R.; Milliron, D. J., Nb-Doped Colloidal $TiO_2$ Nanocrystals with Tunable Infrared Absorption. *Chem. Mater.* **2013**, *25*, 3383-3390.

7. Hirano, M.; Ichihashi, Y., Phase Transformation and Precipitation Behavior of Niobium Component Out of Niobium-Doped Anatase-Type $TiO_2$ Nanoparticles Synthesized Via Hydrothermal Crystallization. *J. Mater. Sci.* **2009**, *44*, 6135-6143.

8. Cottineau, T.; Bealu, N.; Gross, P.-A.; Pronkin, S. N.; Keller, N.; Savinova, E. R.; Keller, V., One Step Synthesis of Niobium Doped Titania Nanotube Arrays to Form (N,Nb) Co-Doped $TiO_2$ with High Visible Light Photoelectrochemical Activity. *J. Mater. Chem. A* **2013**, *1*, 2151-2160.

9. Pittman, R. M.; Bell, A. T., Raman Studies of the Structure of Niobium Oxide/Titanium Oxide ($Nb_2O_5/TiO_2$). *J. Phys. Chem.* **1993**, *97*, 12178-12185.

10. Barshilia, H. C.; Rajam, K. S., A Raman-Scattering Study on the Interface Structure of Nanolayered TiAlN/TiN and TiN/NbN Multilayer Thin Films Grown by Reactive DC Magnetron Sputtering. *J. Appl. Phys.* **2005**, *98*, 0143111-0143119.

11. Guo, Q.; Xie, Y.; Wang, X.; Lv, S.; Hou, T.; Bai, C., Synthesis of Uniform Titanium Nitride Nanocrystalline Powders *via* a Reduction–Hydrogenation–Dehydrogenation–Nitridation Route. *J. Am. Ceram. Soc.* **2005**, *88*, 249-251.

12. Vasu, K.; Gopikrishnan, G. M.; Ghanashyam Krishna, M.; Padmanabhan, K. A., Optical Reflectance, Dielectric Functions and Phonon-Vibrational Modes of Reactively Sputtered Nb-Substituted TiN Thin Films. *Appl. Phys. A* **2012**, *108*, 993-1000.